ISSN 0020-1685, Inorganic Materials, 2009, Vol. 45, No. 5, pp. 568–573. © Pleiades Publishing, Ltd., 2009.
Original Russian Text © S.K. Korchagina, S.A. Ivanov, V.Yu. Proidakova, S.N. Rush, L.F. Rybakova, N.V. Sadovskaya, 2009, published in Neorganicheskie Materialy, 2009, Vol. 45, No. 5, pp. 626–631.

Synthesis, Structure, and Properties of Solid Solutions Based on Bismuth Ferrite

S. K. Korchagina, S. A. Ivanov, V. Yu. Proidakova, S. N. Rush, L. F. Rybakova, and N. V. Sadovskaya

Karpov Scientific and Research Institute of Physics and Chemistry, Moscow, Russia
korchagina@cc.nifhi.ac.ru

Received July 11, 2007

Abstract—Solid solutions of $Bi_{1-x}Pb_xFe_{1-x}Zr_xO_3$ ($x = 0.1$–0.2) are synthesized by the methods of liquid-phase and modified solid-phase synthesis. Also, solid solutions of $[Bi_{0.9}(Pb_{0.9}Ln_{0.1})_{0.1}][Fe_{0.9}(Zr_{0.65}Ti_{0.35})_{0.1}]O_3$, and $[Bi_{0.9}(Pb_{0.9}Ln_{0.1})_{0.1}][Fe_{0.9}(Zr_{0.53}Ti_{0.47})_{0.1}]O_3$ (Ln – La, Pr, Gd, Yb) are made, including synthesis of their precursors with organic ligands. Comprehensive investigations involving thermal analysis, IR spectroscopy, X-ray powder diffraction, atomic force microscopy, dielectric and magnetic measurements, and neutron powder diffraction are performed. The full-profile analysis of X-ray and neutron diffraction patterns by the Rietveld method shows that, over the whole temperature interval of 10–700 K under study, the $Bi_{0.9}Pb_{0.1}Fe_{0.9}Zr_{0.1}O_3$ and $Bi_{0.8}Pb_{0.2}Fe_{0.8}Zr_{0.2}O_3$ compounds are characterized by the perovskite structure (space group $R3c$). The magnetic measurements reveal an antiferromagnetic phase transition in the $Bi_{0.9}Pb_{0.1}Fe_{0.9}Zr_{0.1}O_3$ and $Bi_{0.8}Pb_{0.2}Fe_{0.8}Zr_{0.2}O_3$ solid solutions. The Néel temperature (T_N) decreases considerably with growing $PbZrO_3$ concentration as compared to the Néel point in pure $BiFeO_3$ ($T_N = 633$ K). The perovskite structure with a hexagonal distortion is found in lanthanide-substituted solid solutions and specific features of the surface morphology of the ceramics are analyzed. The magnetic measurements suggest the presence of an antiferromagnetic phase transition in the solid solutions under study, with a considerable drop of T_N in the Ln-alloyed compound as compared to the T_N value in pure $BiFeO_3$

DOI: 10.1134/S0020168509050197

INTRODUCTION

Bismuth ferrite forms the basis of new magnetoelectrical materials used in information recording and storage systems [1] since it provides record-high temperatures of ferroelectric ($T_C = 1083$ K) and magnetic ($T_N = 633$ K) ordering. Structural, ferroelectric, dielectric, and magnetic properties of $BiFeO_3/Pb(Zr_{0.5}Ti_{0.5})O_3$ films made by the method of chemical deposition were studied in [2]. Later, investigators [3] analyzed structural and electrical properties of $(Bi_{1-x}Pb_x)(Fe_{1-x}Zr_{0.6x}Ti_{0.4x})O_3$ ($x = 0.15, 0.25, 0.40, 0.50$) solid solutions synthesized by the mechanochemical activation method.

It was inferred [7] that temperatures of ferroelectric and antiferromagnetic transitions tend to decrease when 10–20% $PbZrO_3$ is added as the second component to bismuth ferrite. Since this problem shows considerable promise, it seems topical and practical to extend the range of starting materials for production of new types of such perovskites, for development and refinement of their synthesis methods, and for looking into their structure and physicochemical properties.

The present study deals with synthesis and analysis of new solid solutions based on bismuth ferrite when they are alloyed with lead zirconate, lead zirconate–titanate (LZT), or LZT with addition of lanthanides for reducing the temperature of the antiferromagnetic phase transition.

EXPERIMENTAL

Synthesis of initial components. Iron oxide Fe_2O_3 (extrapure grade) and lead carbonate $PbCO_3$ (reagent grade) were used as the initial components. Lanthanum (III) acetate $La(CH_3COO)_3 \cdot 3H_2O$, praseodymium acetate $Pr(CH_3COO)_3$, gadolinium (III) acetate $Gd(CH_3COO)_3 \cdot 3H_2O$, and ytterbium acetate $Yb(CH_3COO)_3 \cdot 4H_2O$ were synthesized from the corresponding oxides or carbonates with an acid by the method [4]. Bismuth acetate $Bi(CH_3COO)_3$ was synthesized by the method [5]. Diacetyl acetonatotitanium dichloride $Ti(C_5H_7O_2)_2Cl_2$ was prepared by the method [6], providing a yield of 90% at the decomposition temperature of 230°C. Zirconium acetylacetonate was synthesized by the method [6], providing a yield of 57% after recrystallization from benzene and vacuum drying; the melting temperature was 194.5–195°C. Zirconium decahydrate acetylacetonate $Zr(C_5H_7O_2)_4 \cdot 10H_2O$ was preferable in the reactions.

Synthesis of solid solutions. $Bi_{1-x}Pb_xFe_{1-x}Zr_xO_3$ solid solutions ($x = 0.1$–0.2) were synthesized by the method [7],

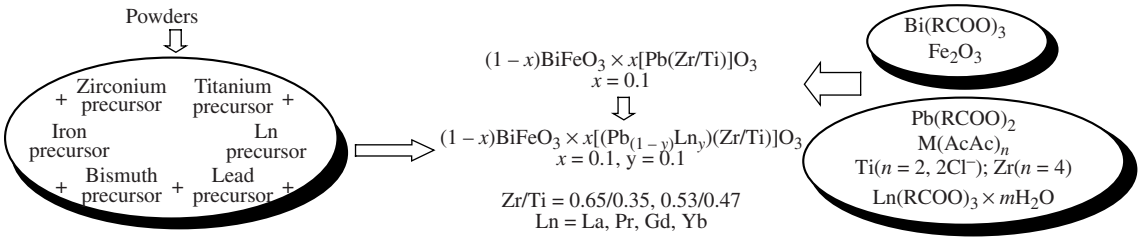

Fig. 1. Scheme for making solid solutions based on bismuth ferrite.

while $[Bi_{0.9}(Pb_{0.9}Ln_{0.1})_{0.1}][Fe_{0.9}(Zr_{0.65}Ti_{0.35})_{0.1}]O_3$ and $[Bi_{0.9}(Pb_{0.9}Ln_{0.1})_{0.1}][Fe_{0.9}(Zr_{0.53}Ti_{0.47})_{0.1}]O_3$ (Ln = La, Pr, Gd, Yb) solid solutions were prepared by the method of modified solid-phase synthesis, which consisted in the use of powdered reagents, such as mixtures of metal oxides with organic and inorganic salts. The charge contained the initial components in an amount sufficient for obtaining a cation stoichiometric mixture, which was calcined at temperatures from room temperature to 600–750°C in Nabertherm furnaces at a heating rate of 2°C/min; the holding time was 2 h.

X-ray phase analysis. The structure, the parameters, and the phase composition of the samples at intermediate synthesis stages were determined according to results of the X-ray phase analysis performed by the powder method with ionization registration of diffraction maxima using a DRON-3 apparatus (CuK_α radiation, $\lambda = 0.1540$ nm, $2\theta = 18°–60°$, the step $\Delta 2\theta = 0.05°$). Additional measurements were performed over a narrow interval of angles $2\theta = 38°–41°$ at a step $\Delta 2\theta = 0.02°$ so as to determine the type of perovskite structure distortion and calculate the lattice parameters.

Morphology of the ceramic. Specific features of the surface morphology of the ceramic were studied in the contact mode of a SOLVER-PRO47 atomic force microscope (NT MDT) with a cantilever made of NSG 10/20 crystal silicon.

Magnetic measurements. The magnetic characteristics of the solid solutions were measured on a Quantum Design SQUID magnetometer in different magnetic fields at temperatures of 5–700 K.[1]

RESULTS AND DISCUSSION

$Bi_{1-x}Pb_xFe_{1-x}Zr_xO_3$ solid solutions ($x = 0.1–0.2$) and previously unstudied $[[Bi_{0.9}(Pb_{0.9}Ln_{0.1})_{0.1}][Fe_{0.9}(Zr_{0.65}Ti_{0.35})_{0.1}]O_3$ solid solutions (L = La, Pr, Gd, Yb) were prepared as shown in the scheme in Fig. 1. This scheme was used to synthesize a group of solid solutions based on bismuth ferrite with addition of 10–20% $PbZrO_3$ and 10% LZT or Ln-alloyed LZT. The analysis of some studies [8, 9] suggested that the physical properties of the solid solutions depended on their synthesis method. The solid-phase synthesis has a drawback in that it is difficult to obtain single-phase materials both before and during calcination. In recent years, both inorganic and organic derivatives have been widely used as the initial compounds. They solve an important problem of a uniform distribution of components in the charge and, hence, the complex oxide material.

The synthesis conditions and the sintering temperatures of the $[Bi_{0.9}(Pb_{0.9}Ln_{0.1})_{0.1}][Fe_{0.9}(Zr_{0.65}Ti_{0.35})_{0.1}]O_3$ (L = La, Pr, Gd, Yb) solid solutions were chosen on the basis of earlier results of thermogravimetric analysis of synthesized $BiFeO_3$, since bismuth ferrite is the main component of the solid solutions under study. The use of the modified solid-phase synthesis allowed the formation temperature of the solid solutions at hand to be reduced to 600°C.

The diffraction patterns of the samples of $[Bi_{0.9}(Pb_{0.9}Ln_{0.1})_{0.1}][Fe_{0.9}(Zr_{0.65}Ti_{0.35})_{0.1}]O_3$ and $[Bi_{0.9}(Pb_{0.9}Ln_{0.1})_{0.1}][Fe_{0.9}(Zr_{0.53}Ti_{0.47})_{0.1}]O_3$ (Ln = La, Pr, Gd, Yb), which were annealed at 600°C, confirmed the formation of perovskite, but included traces of $Bi_{36}Fe_2O_{57}$ and $Bi_2Fe_4O_9$ impurity phases.

The unit cell parameters for the compositions under study are given in the table. All the compounds retained a typical "perovskite" structure with hexagonal distortion. The volume of the crystal lattice of the $[Bi_{0.9}(Pb_{0.9}Ln_{0.1})_{0.1}][Fe_{0.9}(Zr_{0.65}Ti_{0.35})_{0.1}]O_3$ solid solutions under study changed. The crystal lattice decreased upon addition of La, but increased with respect to the $[Bi_{0.9}Pb_{0.1}][Fe_{0.9}(Zr_{0.65}Ti_{0.35})_{0.1}]O_3$ solid solution as Pr, Gd, and Yb were added. The crystal lattice of $[Bi_{0.9}(Pb_{0.9}Ln_{0.1})_{0.1}][Fe_{0.9}(Zr_{0.53}Ti_{0.47})_{0.1}]O_3$ increased monotonically upon addition of La, Pr and Gd, but increased sharply with respect to the $[Bi_{0.9}Pb_{0.1}][Fe_{0.9}(Zr_{0.53}Ti_{0.47})_{0.1}]O_3$ solid solution upon alloying with Yb.

The microstructures of the undoped $[Bi_{0.9}Pb_{0.1}][Fe_{0.9}(Zr_{0.53}Ti_{0.47})_{0.1}]O_3$ and $[Bi_{0.9}Pb_{0.1}][Fe_{0.9}(Zr_{0.65}Ti_{0.35})_{0.1}]O_3$ are shown in Fig. 2. It is seen from the microphotographs that the morphology of the ceramic changed little with the molar ratio of Zr and Ti ions. Oriented scaly crystals with a lateral dimension of 0.5 to 1 μm, which grew as mutually parallel layers, were observed in both cases. Furthermore,

[1] The magnetic measurements were performed at the Angstrom Laboratory, Uppsala University, Sweden.

Calculated parameters of a unit cell of $BiFeO_3$-based solid solutions

Composition	*a*, Å	*c*, Å	*c*/*a*	ω	*V*, Å^3
$Bi_{0.9}Pb_{0.1}Fe_{0.9}Zr_{0.1}O_3$	5.6116(7)	13.921	2.48	9°43′	379.653
$Bi_{0.8}Pb_{0.2}Fe_{0.8}Zr_{0.2}O_3$	5.6447(7)	13.991	2.47	8°83′	386.104
$[Bi_{0.9}Pb_{0.1}][Fe_{0.9}(Zr_{0.65}Ti_{0.35})_{0.1}]O_3$	5.5367(3)	13.7502	2.4835	9°49′	365.041
$[Bi_{0.9}(Pb_{0.9}La_{0.1})_{0.1}][Fe_{0.9}(Zr_{0.65}Ti_{0.35})_{0.1}]O_3$	5.5350(3)	13.7452	2.4833	9°47′	363.684
$[Bi_{0.9}(Pb_{0.9}Pr_{0.1})_{0.1}][Fe_{0.9}(Zr_{0.65}Ti_{0.35})_{0.1}]O_3$	5.5940(3)	13.8776	2.4808	9°11′	376.088
$[Bi_{0.9}(Pb_{0.9}Gd_{0.1})_{0.1}][Fe_{0.9}(Zr_{0.65}Ti_{0.35})_{0.1}]O_3$	5.5879(3)	13.8723	2.4826	9°37′	375.125
$[Bi_{0.9}(Pb_{0.9}Yb_{0.1})_{0.1}][Fe_{0.9}(Zr_{0.65}Ti_{0.35})_{0.1}]O_3$	5.5911(3)	13.8847	2.4833	9°47′	375.891
$[Bi_{0.9}Pb_{0.1}][Fe_{0.9}(Zr_{0.53}Ti_{0.47})_{0.1}]O_3$	5.5350(3)	13.7452	2.4833	9°46′	349.926
$[Bi_{0.9}(Pb_{0.9}La_{0.1})_{0.1}][Fe_{0.9}(Zr_{0.53}Ti_{0.47})_{0.1}]O_3$	5.5286(3)	13.7144	2.4806	9°08′	363.026
$[Bi_{0.9}(Pb_{0.9}Pr_{0.1})_{0.1}][Fe_{0.9}(Zr_{0.53}Ti_{0.47})_{0.1}]O_3$	5.5298(3)	13.7260	2.4822	9°31′	363.491
$[Bi_{0.9}(Pb_{0.9}Gd_{0.1})_{0.1}][Fe_{0.9}(Zr_{0.53}Ti_{0.47})_{0.1}]O_3$	5.5363(3)	13.7315	2.4807	9°10′	364.360
$[Bi_{0.9}(Pb_{0.9}Yb_{0.1})_{0.1}][Fe_{0.9}(Zr_{0.53}Ti_{0.47})_{0.1}]O_3$	5.5675(3)	13.8204	2.4823	9°33′	370.998

rounded grains 50 to 250 nm in size were observed and these grains were spaced apart (50–150 nm) in $[Bi_{0.9}Pb_{0.1}][Fe_{0.9}(Zr_{0.53}Ti_{0.47})_{0.1}]O_3$ or formed aggregates made up of more than ten grains in $[Bi_{0.9}Pb_{0.1}][Fe_{0.9}(Zr_{0.65}Ti_{0.35})_{0.1}]O_3$.

The microstructure of the ceramics of the unalloyed solutions changed considerably after addition of the rare-earth elements. Figure 3 presents AFM images of the surface of the $[[Bi_{0.9}(Pb_{0.9}Ln_{0.1})_{0.1}][Fe_{0.9}(Zr_{0.53}Ti_{0.47})_{0.1}]O_3$ (Ln = La, Gd, Yb, Pr) solid solution ceramic. Unlike in the initial solid solution, scaly forms disappeared after addition of the alloying elements and were replaced by micrograins 0.5 to 1.5 μm in size having different habits and nanograins 30 to 100 nm in size. In some cases, aggregates comprising several dozen to several hundred nanograins (Fig. 3c) were formed, while the micrograins could have a substructure, i.e., consisting of nanograins (Fig. 3b). Alloying of the $[Bi_{0.9}Pb_{0.1}][Fe_{0.9}(Zr_{0.65}Ti_{0.35})_{0.1}]O_3$ solid solution led to similar changes in the surface structure (Fig. 4). Thus, the microstructure of the $[Bi_{0.9}Pb_{0.1}][Fe_{0.9}(Zr_{0.53}Ti_{0.47})_{0.1}]O_3$ and $[Bi_{0.9}Pb_{0.1}][Fe_{0.9}(Zr_{0.65}Ti_{0.35})_{0.1}]O_3$ ceramics was almost independent of the molar ratio of Zr and Ti ions, while alloying with La, Pr, Gd, and Yb caused considerable morphological changes in the microstructure.

The magnetic measurements revealed an antiferromagnetic phase transition in the $Bi_{1-x}Pb_xFe_{1-x}Zr_xO_3$ (x = 0.1–0.2) solid solutions. It was found that the Néel temperature tended to decrease with growing concentration of $PbZrO_3$ as compared to pure $BiFeO_3$. T_N, which was equal to 643 K in pure $BiFeO_3$, decreased after addition of Ln. For example, T_N decreased to 610 K (Fig. 5) and to 600 K (Fig. 6) after addition of lantha-

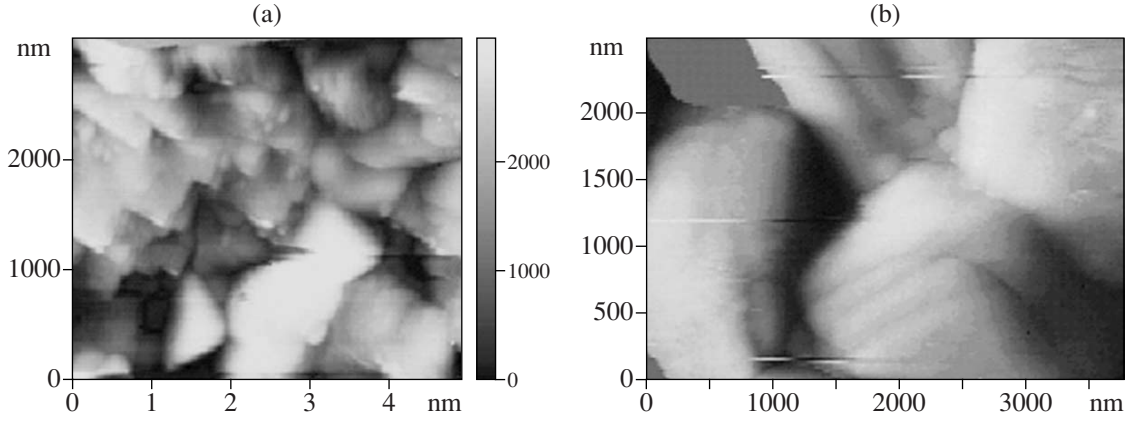

Fig. 2. AFM images of the surface of the ceramics of the unalloyed solid solutions: $[Bi_{0.9}Pb_{0.1}][Fe_{0.9}(Zr_{0.53}Ti_{0.47})_{0.1}]O_3$ (a), $[Bi_{0.9}Pb_{0.1}][Fe_{0.9}(Zr_{0.65}Ti_{0.35})_{0.1}]O_3$ (b).

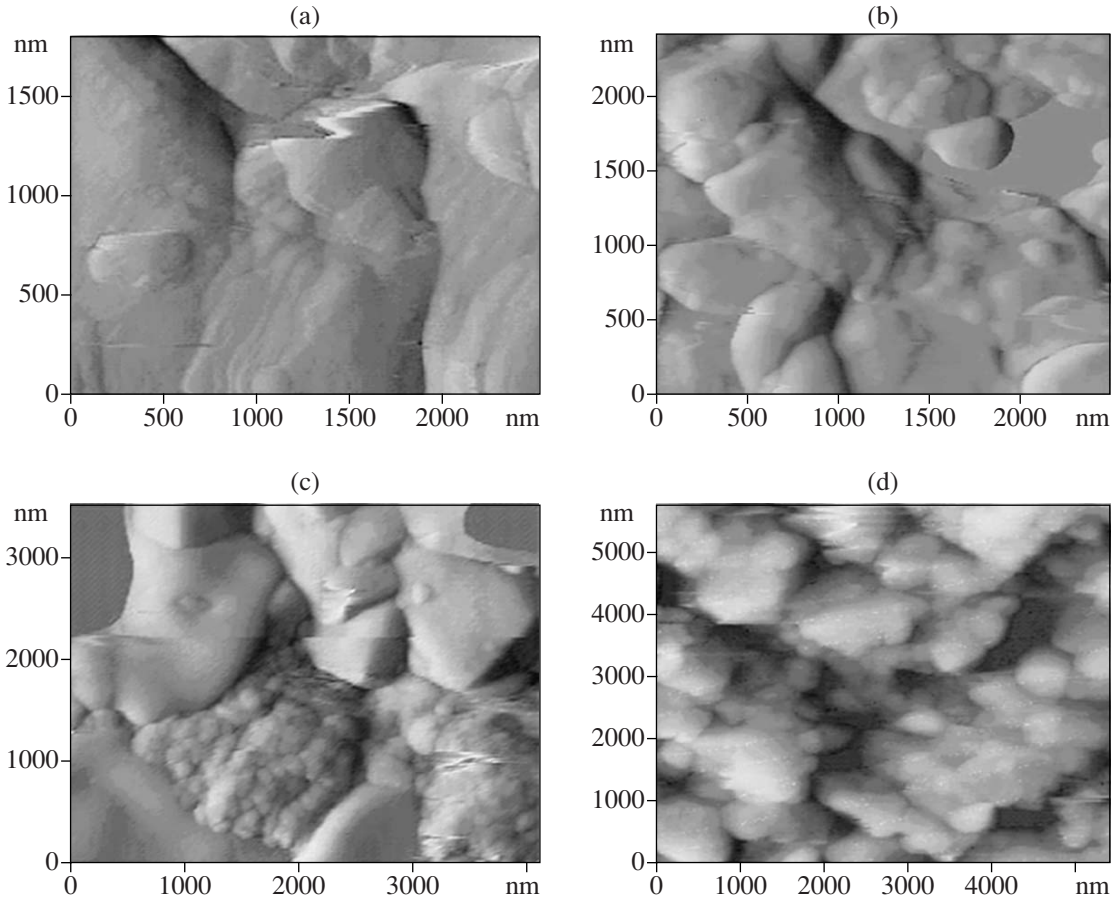

Fig. 3. AFM images of the surface of the solid solution ceramics with additions: (a) $[Bi_{0.9}(Pb_{0.9}La_{0.1})_{0.1}][Fe_{0.9}(Zr_{0.53}Ti_{0.47})_{0.1}]O_3$ (b) $[Bi_{0.9}(Pb_{0.9}Gd_{0.1})_{0.1}][Fe_{0.9}(Zr_{0.53}Ti_{0.47})_{0.1}]O_3$ (c) $[Bi_{0.9}(Pb_{0.9}Yb_{0.1})_{0.1}][Fe_{0.9}(Zr_{0.53}Ti_{0.47})_{0.1}]O_3$ (d) $[[Bi_{0.9}(Pb_{0.9}Pr_{0.1})_{0.1}][Fe_{0.9}(Zr_{0.53}Ti_{0.4})_{0.1}]O_3$.

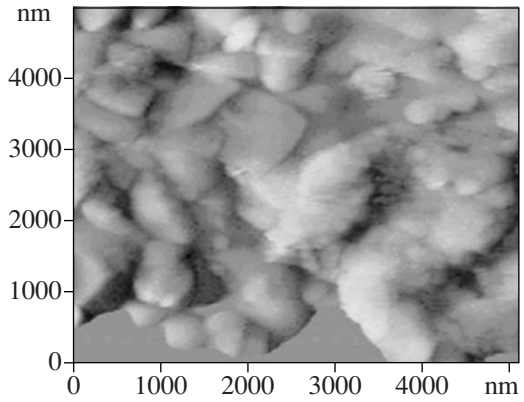

Fig. 4. AFM image of the surface of the $[Bi_{0.9}(Pb_{0.9}Pr_{0.1})_{0.1}][Fe_{0.9}(Zr_{0.65}Ti_{0.35})_{0.1}]O_3$ solid solution ceramic.

num (1%) and praseodymium (1%) respectively. The greatest effect was observed for the compounds with ytterbium (1%), in which T_N decreased the most and was equal to 570 K (Fig. 7). The temperature dependences of the magnetization for the gadolinium-doped compounds suggested the presence of two anomalies at

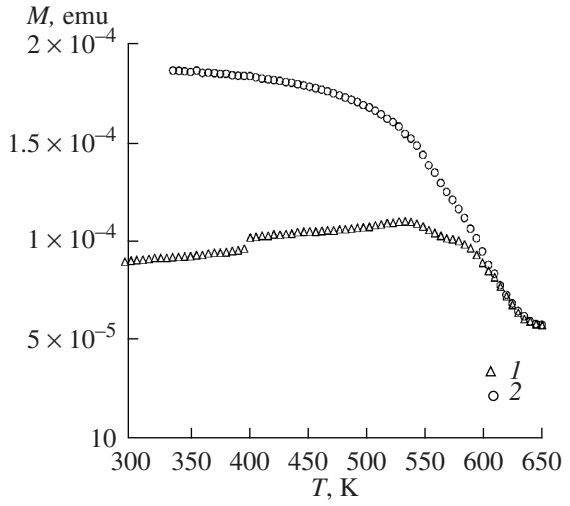

Fig. 5. Temperature dependences of the magnetization of the $[Bi_{0.9}$ $(Pb_{0.9}La_{0.1})_{0.1}][Fe_{0.9}$ $(Zr_{0.53}Ti_{0.47})_{0.1}]O_3$ solid solution (*1*) without and (*2*) with a magnetic field applied, H = 80 kOe/m.

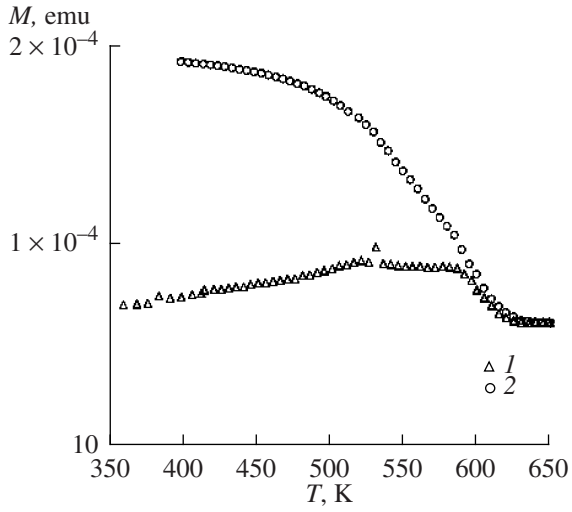

Fig. 6. Temperature dependences of the magnetization of the $[Bi_{0.9}(Pb_{0.9}Pr_{0.1})_{0.1}]$ $[Fe_{0.9}(Zr_{0.53}Ti_{0.47})_{0.1}]O_3$ solid solution (for *1* and *2*, see the caption of Fig. 5).

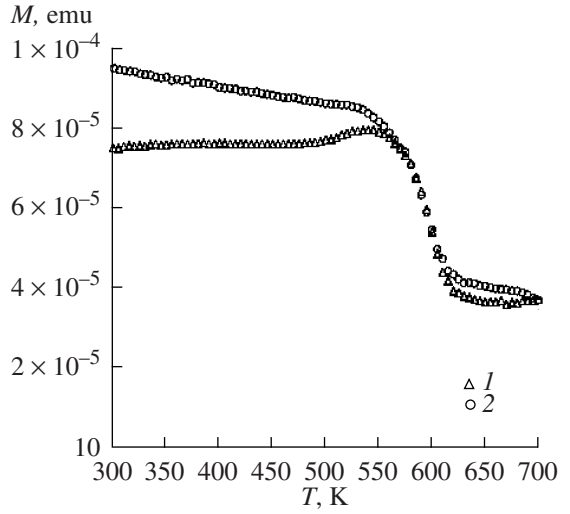

Fig. 7. Temperature dependences of the magnetization of the $[Bi_{0.9}(Pb_{0.9}Yb_{0.1})_{0.1}][Fe_{0.9}(Zr_{0.53}Ti_{0.47})_{0.1}]O_3$ solid solution (for *1* and *2*, see the caption of Fig. 5).

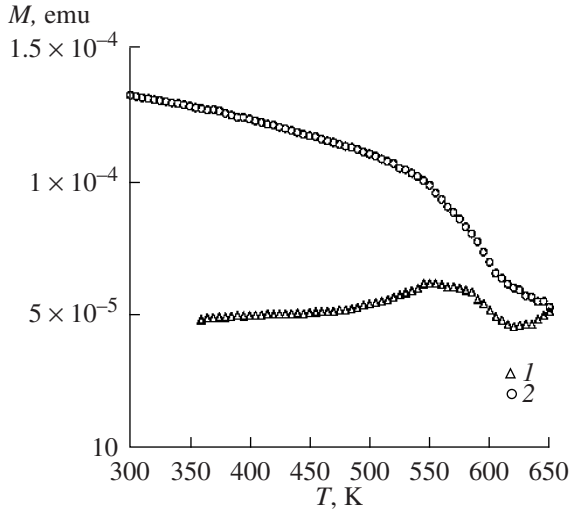

Fig. 8. Temperature dependences of the magnetization of the $[Bi_{0.9}(Pb_{0.9}Gd_{0.1})_{0.1}][Fe_{0.9}(Zr_{0.53}Ti_{0.47})_{0.1}]O_3$ solid solution (for *1* and *2*, see the caption of Fig. 5).

580 and 650 K, which were probably due to the inhomogeneity of the test sample (Fig. 8). All the Ln-doped compounds retained the antiferromagnetic character of their properties.

CONCLUSIONS

A highly efficient method has been proposed for synthesis of $[[Bi_{0.9}(Pb_{0.9}Ln_{0.1})_{0.1}][Fe_{0.9}(Zr_{0.65}Ti_{0.35})_{0.1}]O_3$ and $[Bi_{0.9}(Pb_{0.9}Ln_{0.1})_{0.1}][Fe_{0.9}(Zr_{0.53}Ti_{0.47})_{0.1}]O_3$ solid solutions with a hexagonally distorted perovskite structure. In this method, metal oxides in the charge are replaced by their organic derivatives.

The microstructure of the $[Bi_{0.9}Pb_{0.1}][Fe_{0.9}(Zr_{0.53}Ti_{0.47})_{0.1}]O_3$ and $[Bi_{0.9}Pb_{0.1}][Fe_{0.9}(Zr_{0.65}Ti_{0.35})_{0.1}]O_3$ solid solution ceramics depended little on the molar ratio of Zr and Ti ions, whereas alloying with La, Gd, Yb, and Pr considerably changed the surface morphology.

The magnetic measurements revealed an antiferromagnetic phase transition in the solid solutions under study, with T_N decreasing markedly after alloying with Ln as compared to the corresponding value in $BiFeO_3$ (T_N = 643 K).

ACKNOWLEDGMENTS

This work was supported by the Russian Foundation for Basic Research (grant no. 06-03-32362).

REFERENCES

1. Woodward, D.I., Reaney, I.M., Eitel, R.E., and Randall, C.A., Crystal and Domain Structure of the $BiFeO_3$–$PbTiO_3$ Solid Solution, *J. Appl. Phys.*, 2003, vol. 94, no. 5, pp. 3313–3318.
2. Li, Y.W., Sun, J.L., Chen, J. et al., Structural, Ferroelectric, Dielectric and Magnetic Properties of $BiFeO_3$/$Pb(Zr_{0.5}Ti_{0.5})O_3$ Multilayer Films Derived by Chemical Solution Deposition, *Appl. Phys. Lett.*, 2005, vol. 87, pp. 182902–1–3.
3. Choudhary, R. N. P., Perez, K., Bhattacharya, P., Katiyar, R.S., Structural and Electrical Properties of $BiFeO_3$–$Pb(ZrTi)O_3$ Composites, *Appl. Phys. A*, 2007, vol. 86, pp. 131–138.
4. Starostina, T.A., Syutkina, O.P., Rybakova, L.F. et al., The Use of Carboxylates for Production of Yttrium-Barium Cuprate in the Form of Powders and Films, *Zh. Neorgan. Khimii*, 1992, vol. 37, no. 11, pp. 2402–2405.
5. Tomashpolskii, Yu.Ya., Rybakova, L.F., Sadovskaya, N.V. et al., Composition, Microstructure, Superconduction and Ferroelectric Properties of Bi–Sr–Ca–Cu–O/Pb–Ti–Zr–O Layered Structures, *Neorgan. Materiali*, 2003, vol. 39, no. 7, pp. 863–871.
6. *Rukovodstvo po neorganicheskomu sintezu* (Handbook of Inorganic Synthesis), Brauer, G.T., Ed., Moscow: Mir, 1985, vol. 4, pp. 1485–1487.
7. Ivanov, S.A., Nordblad, P., Tellgren, R. et al. Influence of $PbZrO_3$ Doping on the Structural and Magnetic Properties of $BiFeO_3$, *Solid State Sci.*, 2008, vol. 10, no. 12, pp. 1875-1885.
8. Ruette, B., Zvygin, S., Pyatakov, A. et al., *Phys. Rev. B*, 2004, vol. 69, p. 064114.
9. Kim, J.K., Kim, S.S., and Kim, W.–J., Sol–Gel Synthesis and Properties of Multiferroic $BiFeO_3$, *Mater. Lett.,* 2005, vol. 59, pp. 4006–4009.